Cross-coupling stiffness for natural goal-directed robot motion

Dennis Ossadnik and Sami Haddadin ⋆

Chair of Robotics and Systems Intelligence (RSI), Munich Institute of Robotics and Machine Intelligence (MIRMI), Technical University of Munich, Germany (e-mail: dennis.ossadnik@tum.de, haddadin@tum.de).

Abstract: The capability of humans to use their natural dynamics for generating explosive motions in a highly-coordinated sequence is a feature that has yet to be reached in robotics. With the introduction of intrinsically elastic joints, great progress towards this goal has been made. However, there are still some challenges associated with this type of actuation, which limits its application. Generating goal-directed sequences has proven to be difficult since optimal control solutions tend to result in uncoordinated swing-up motions. This can be explained when viewing the structure of the stiffness matrix: If the elastic elements are placed in series with the motor, a diagonal stiffness matrix is generated. This in turn leads to a multitude of frequencies in which the system can oscillate. By adding off-diagonal elements, a dominant main resonance behavior can be achieved. Leveraging this cross-coupling stiffness, we show that robots are capable to produce natural goal-directed oscillatory motions as well as explosive movements that closely resemble human throwing.

Keywords: Robot manipulators; Optimal control; Vibration and modal analysis

1. INTRODUCTION

For a number of decades, there have been various endeavors to exploit intrinsic joint elasticity in the robotics community (e.g. Grebenstein et al. (2011); Ugurlu et al. (2014)). The resulting systems reach high performance in terms of the reachable output power and energy efficiency. In the case of *Series Elastic Actuators* (SEA), a spring is placed in series with the motor. By optimally storing and releasing potential energy in springs, these systems can significantly outperform rigid actuators (cf. Haddadin et al. (2009)). The timing of energy storage and release, however, could not yet be controlled well. Motion plans generated by optimal control often result in resonant excitation signals.

With the introduction of *Variable Stiffness Actuators* (VSA), controlled energy transfer between bodies is possible for some well-timed solutions, leading to a goal-directed launch sequence (cf. Haddadin et al. (2012)). However, this comes at unreasonable costs in terms of control: The computational complexity of the problem is quite high, which makes it challenging to obtain real-time optimal control solutions (cf. Haddadin et al. (2016)).

Clutched elastic actuators (CEA, cf. Plooij et al. (2017)) aim to control the energy flow by leveraging clutches in the drive train (cf. Ossadnik et al. (2022); Rouse et al. (2014)). Regardless, the discrete nature of the clutch engagement again increases the control complexity.

⋆ We gratefully acknowledge the funding support of the European Union's Horizon 2020 research and innovation programme as part of the project Darko under grant no. 101017274. Please note that Sami Haddadin has a potential conflict of interest as a shareholder of Franka Emika GmbH.

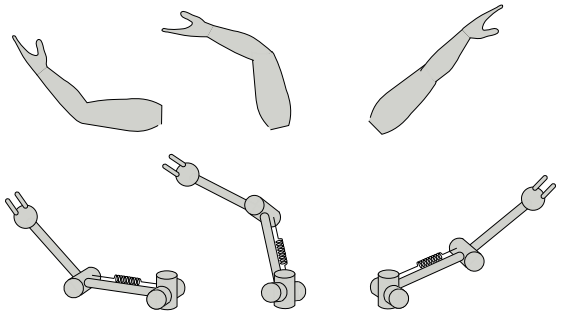

Fig. 1. Sketch of a throwing motion for a human and a robotic arm. Using a cross-coupling stiffness, the dynamics of the robotic arm are reshaped such that goal-directed explosive movements naturally occur.

This is in stark contrast to the human musculoskeletal system. Notwithstanding the limited bandwidth and high delays, humans are highly capable of accomplishing complex motion sequences. During throwing movements, the entire kinematic chain from the foot to the throwing hand is involved. Professional athletes are able to precisely coordinate each segment such that all joints reach their maximum velocity one after another. In this acceleration phase, the velocity is drastically increased from the proximal to the distal elements of the chain. This is known as *proximo-distal sequence* in the biomechanics literature (cf. Heger and Wank (2021)). There clearly exists a gap between what has been achieved in robotics so far and what can be observed in biological systems.

We hypothesize that the issue lies within the very structure of the system itself. The human arm is comprised of multiarticular coupling stiffnesses. If these stiffnesses are well-tuned, coordinated motions could be achieved by means of natural dynamics alone. Usually, such coupling terms are missing in elastic joint robots. In a robot equipped with SEAs, for instance, a diagonal stiffness matrix is created. Without any control input, the resulting systems behave chaotically due to the many frequencies that the system can oscillate with. It has been observed (cf. Haddadin et al. (2012)) that by adding off-diagonal elements to the stiffness matrix, the dynamics of these systems can be reshaped in a desirable manner: The coupling terms can be chosen to achieve a single dominant resonance behavior. The human musculoskeletal system might therefore implement cross-coupling which then can be exploited easily by the brain and the central nervous system.

1.1 Contribution

In this paper, we show that cross-coupling stiffness can be leveraged to enhance the performance of elastic joint robots. In a series of hardware experiments with a lightweight robot, we show that using a virtual cross-coupling stiffness

- The coupled system always moves in a closed orbit.
- Periodic motions can be taught intuitively by moving the robot in the desired direction (in contrast to a system with only diagonal stiffnesses).

To further evaluate the concept, we conduct an optimal control study in which we compare an elastic double pendulum and a shoulder/elbow system with and without coupling stiffness. The results demonstrate that

- We are able to control the energy flow from the proximal to the distal parts of the chain, achieving a goal-directed launch sequence similar to human throwing.
- We avoid unwanted resonant excitation typically associated with series elastic actuation.

1.2 Organization

In Section 2, we begin with a brief overview of how to select an appropriate cross-coupling stiffness. Using a virtual cross-coupling stiffness, we show the results of hardware experiments in Section 3. Then, in Section 4, we proceed to formulate the optimal control for generating explosive movements for a fully elastic robot. The simulation results are given in Section 5 before concluding the paper in Section 6.

2. CROSS-COUPLING STIFFNESS

First, let us consider a robot in the absence of Coriolis, centrifugal and gravitational terms. The dynamics of this system can be stated as

$$\boldsymbol{M}(\boldsymbol{q})\ddot{\boldsymbol{q}} + \boldsymbol{K}(\boldsymbol{q} - \boldsymbol{q}_0) = \boldsymbol{0}, \tag{1}$$

where $\boldsymbol{q}$ is the vector of link positions, $\boldsymbol{q}_0$ is an initial configuration, $\boldsymbol{M}(\boldsymbol{q})$ is the inertia matrix and $\boldsymbol{K}$ is an arbitrary, yet-to-be-defined, positive-definite stiffness matrix. We assume that solutions to Eq. (1) can be expressed as

$$\boldsymbol{q}(t) = \sum_{i=1}^{n} a_i \boldsymbol{\zeta}_i e^{\jmath \omega_i t}, \tag{2}$$

with amplitudes a_i and frequencies $\omega_i > 0$, which leads to the the generalized eigenvalue problem (cf. Petit et al. (2012))

$$\lambda_i \boldsymbol{M}(\boldsymbol{q})\boldsymbol{\zeta}_i = \boldsymbol{K}\boldsymbol{\zeta}_i \tag{3}$$

where $\lambda_i = \omega_i^2$ and $\{\lambda_i, \boldsymbol{\zeta}_i\}$ denotes the set of eigenvalue-eigenvector pairs, the *eigenmodes* of the system. We wish to shape the eigenmodes such that n repeated eigenvalues λ_s arise (cf. Petit et al. (2012); Haddadin et al. (2012)). Presupposing there is only a single eigenvalue, we can reformulate the generalized eigenvalue problem as

$$\lambda_s \boldsymbol{M}(\boldsymbol{q})\boldsymbol{V} = \boldsymbol{K}\boldsymbol{V}, \tag{4}$$

where $\boldsymbol{V} = [\boldsymbol{\zeta}_1, \dots \boldsymbol{\zeta}_n]$. It follows that

$$\boldsymbol{K} = \boldsymbol{K}(\boldsymbol{q}) = \lambda_s \boldsymbol{M}(\boldsymbol{q}). \tag{5}$$

Therefore, for producing the desired behavior, a configuration-dependent stiffness matrix must be chosen that corresponds to the scaled mass matrix.

2.1 Oscillatory behaviour

We now proceed to analyze the oscillatory behavior of a double pendulum equipped with cross-coupling stiffness. We chose the same mechanical parameters as in Haddadin et al. (2012). They are summarized in Table 1. For comparison, we also simulate the same system with a diagonal stiffness only.

The phase plot in Figure 2 shows the evolution of both systems, which are initialized at the equilibrium configuration with some initial velocity. The curve traced by the coupled system is elliptical, forming a closed periodic orbit. This synchronous kind of motion is generated solely by the natural dynamics of the system. With the choice of stiffness matrix, there is but a single main resonance

Table 1. Mechanical parameters of the double pendulum system

Parameter	Symbol	Value
Mass Link 1	m_1	5 kg
Mass Link 2	m_2	4.6 kg
Moment of Inertia Link 1	J_{l_1}	0.0453 kg m^2
Moment of Inertia Link 2	J_{l_2}	0.0492 kg m^2
Length Link 1	l_1	0.34 m
Length Link 2	l_2	0.34 m

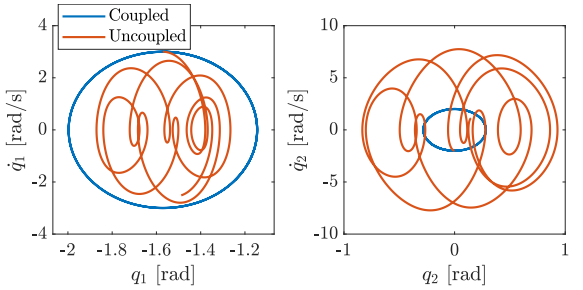

Fig. 2. Phase plots for the elastic double pendulum. The system is initialized at $\boldsymbol{q} = [0, 0]^\mathsf{T}$, $\dot{\boldsymbol{q}} = [3, -2]^\mathsf{T}$.

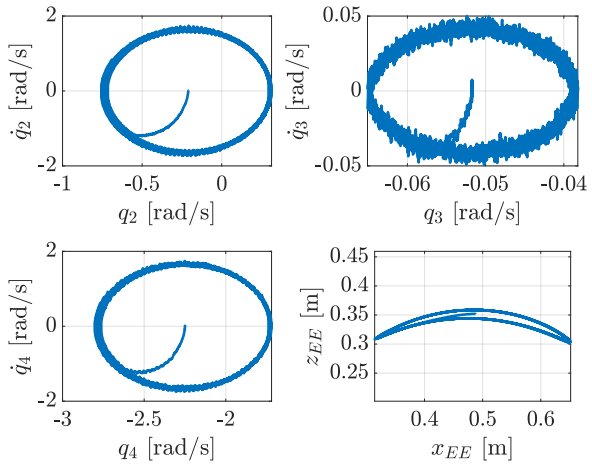

Fig. 3. Coupled system. Phase plots and end-effector position after a push in the x-direction.

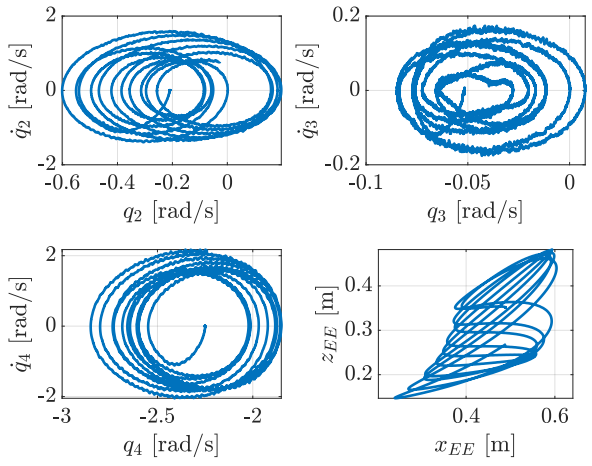

Fig. 4. Uncoupled system. Phase plots and end-effector position after a push in the x-direction.

behavior. Contrary to that, the uncoupled system exhibits multiple frequencies. The resulting motion can be characterized as a non-periodic chaotic type of motion. In the small simulation time frame, already a large portion of the phase space is covered.

3. HARDWARE EXPERIMENTS

Cross-coupling can also be exploited when dealing with more complex systems. We use the Franka Emika Panda to implement a virtual cross-coupling system. The dynamics of this system can be written as

$$\boldsymbol{M}(\boldsymbol{q})\ddot{\hat{\boldsymbol{q}}} + \boldsymbol{K}(\boldsymbol{q})(\hat{\boldsymbol{q}} - \hat{\boldsymbol{q}}_0) = \boldsymbol{\tau}_{ext}. \tag{6}$$

Here, $\hat{\boldsymbol{q}}$ corresponds to the virtual joint position and $\boldsymbol{\tau}_{ext}$ refers to the measured external torques. To match the actual robot's motion with the virtual system, we set the current joint velocity of the virtual system as a desired joint velocity

$$\dot{\boldsymbol{q}}_{des} = \int \boldsymbol{M}^{-1}(\boldsymbol{q})\left(\boldsymbol{\tau}_{ext} - \boldsymbol{K}(\boldsymbol{q})(\hat{\boldsymbol{q}} - \hat{\boldsymbol{q}}_0)\right) \mathrm{d}t. \tag{7}$$

This is then passed to the robots' joint velocity control interface. Closed orbits can now be easily encoded by leveraging the torque-sensing capability of the robot.

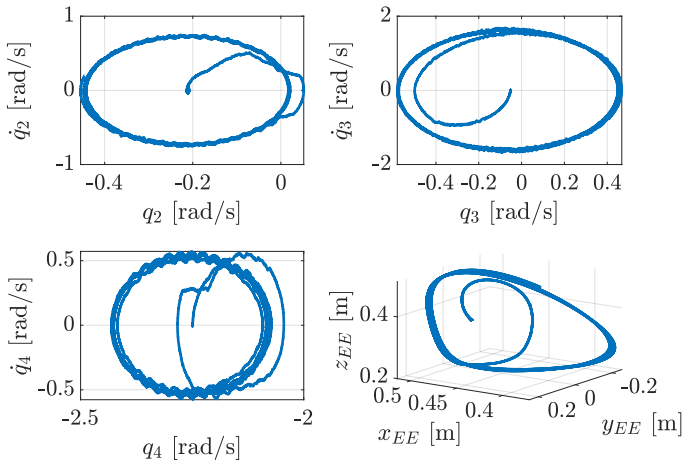

Fig. 5. Coupled system. Phase plots and end-effector position after guiding the robot on an elliptical curve.

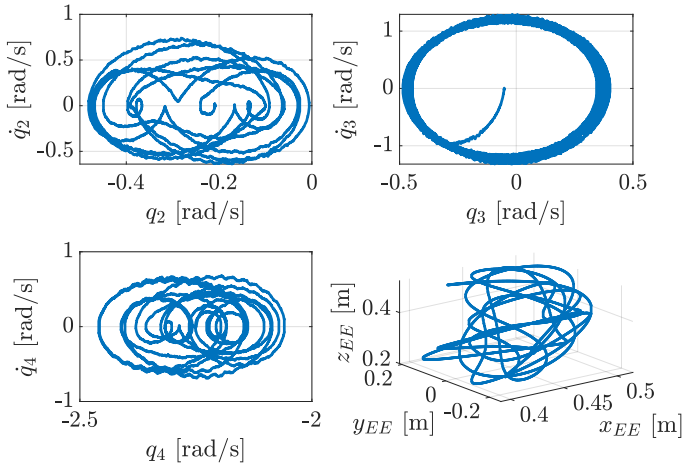

Fig. 6. Uncoupled system. Phase plots and end-effector position after guiding the robot on an elliptical curve.

3.1 Programming closed orbits

To program closed orbits, we just have to start the controller at an equilibrium position and use the robot's sense of touch to initialize the motion. Generating directed behaviors becomes very natural and intuitive. Similar to a slingshot, the robot's end-effector can be drawn back and released. The end-effector will then move along a vector that is opposite to the drawing direction. In the following, we compare coupled system equipped with cross-coupling stiffness and an uncoupled system with a diagonal stiffness matrix [1] .

3.2 Pushing along a straight line

In the first hardware experiment, we excite the robot by pushing along a straight line in the approximate x-direction of the end-effector. Figures 3 and 4 shows the experimental results for the coupled and the uncoupled system, respectively. In the case of the coupled system, closed orbits arise for all three joints. The robot moves

[1] The desired eigenvalue is set to $\lambda_s = 10$ and all the diagonal elements of the uncoupled system are set to 10 as well. For the experiments, only joints 1, 2, and 4 are used.

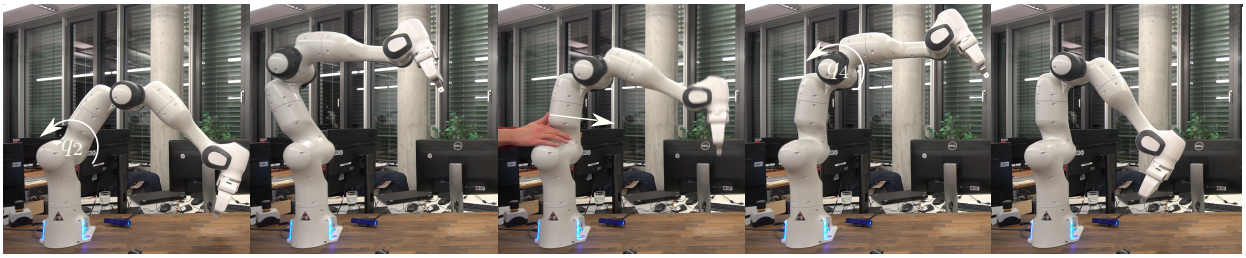

Fig. 7. Picture series of the energy transfer experiment.

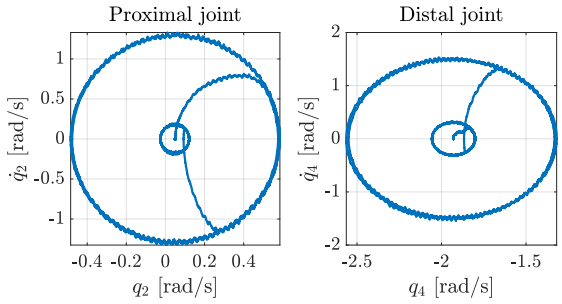

Fig. 8. Phase plots for the energy transfer experiment.

along the "taught" line with a slight movement in the z-direction as well. There is no such coordination in the uncoupled system case.

3.3 Guiding along an elliptical curve

Similarly, elliptical motions can be taught by hand-guiding the robot alongside the desired curve. Figures 5 and 6 show the trials for the coupled and uncoupled systems, respectively. For the coupled system, a periodic approximate ellipse can be "entrained". This shape is not visible in the uncoupled system, although joint 3 forms a closed periodic orbit.

3.4 Energy transfer

In the last experiment, we investigate how to transfer energy from proximal to distal joints. For this, we consider the motion of joints 2 and 4 only. First, we excite the robot such that the motion is dominated by q_2. Then, by holding the first joint at the right time, we inject energy into the second joint (cf. Figures 8 and 7) After the transfer, the oscillation is dominated by the distal joint q_4. Thus, using the coupling stiffness, transferring energy between joints can be intuitively controlled.

The experiments demonstrate the potential for the application of cross-coupling stiffness in the generation of natural, goal-directed behavior. We will now show how this can be utilized in the generation of explosive motions in an optimal control setting.

4. GENERATION OF EXPLOSIVE MOVEMENTS

In this section, we aim to generate optimal throwing motions by leveraging cross-coupling in fully elastic joint robots. We consider two systems: A 2-DoF double pendulum and a 3-DoF shoulder arm system (cf. Figure 9).

4.1 Full system model

First, let us consider the full dynamics of an elastic joint robot under the simplifying assumption that motor and robot dynamics are coupled only via the springs (cf. Spong (1989)). We introduce motor positions $\boldsymbol{\theta}$ to formulate the robot dynamics

$$\boldsymbol{M}(\boldsymbol{q})\ddot{\boldsymbol{q}} + \boldsymbol{C}(\boldsymbol{q},\dot{\boldsymbol{q}})\dot{\boldsymbol{q}} + \boldsymbol{g}(\boldsymbol{q}) + \boldsymbol{K}(\boldsymbol{q}-\boldsymbol{\theta}) = \boldsymbol{0} \tag{8}$$

$$\boldsymbol{B}\ddot{\boldsymbol{\theta}} + \boldsymbol{K}(\boldsymbol{\theta}-\boldsymbol{q}) = \boldsymbol{\tau}. \tag{9}$$

Here, $\boldsymbol{C}(\boldsymbol{q},\dot{\boldsymbol{q}})\dot{\boldsymbol{q}}$ are the Coriolis and centrifugal terms, $\boldsymbol{g}(\boldsymbol{q})$ is the gravity vector, and $\boldsymbol{B}$ is the motor inertia. In the following, we assume that the stiffness matrix is constant, i.e.

$$\boldsymbol{K} = \lambda_s \boldsymbol{M}(\boldsymbol{q}_0), \tag{10}$$

for an equilibrium position $\boldsymbol{q}_0$. As in Haddadin et al. (2012), we aim to maximize the end-link velocity of the considered elastic robot arm. To formulate the optimal control problem, we assume that the dynamics in Eq. (8) is in singular perturbation form: Given a control law $\boldsymbol{\tau} = \boldsymbol{K}_P(\dot{\boldsymbol{\theta}}_d - \dot{\boldsymbol{\theta}})$, where $\boldsymbol{K}_P$ is a diagonal matrix, we can rewrite the motor dynamics as (cf. Haddadin et al. (2012))

$$\boldsymbol{\epsilon}(\boldsymbol{B}\ddot{\boldsymbol{\theta}} + \boldsymbol{K}(\boldsymbol{\theta}-\boldsymbol{q})) = \dot{\boldsymbol{\theta}}_d - \dot{\boldsymbol{\theta}}, \tag{11}$$

where $\boldsymbol{\epsilon} = \boldsymbol{K}_P^{-1}$. Taking the limit $\boldsymbol{\epsilon} \to \boldsymbol{0}$ leads to $\dot{\boldsymbol{\theta}} = \dot{\boldsymbol{\theta}}_d$. Now, we can restate the dynamics as

$$\dot{\boldsymbol{x}} = \boldsymbol{f}(\boldsymbol{x},\boldsymbol{u}) := \begin{bmatrix} \boldsymbol{u} \\ \dot{\boldsymbol{q}} \\ \boldsymbol{M}(\boldsymbol{q})^{-1}(-\boldsymbol{h}(\boldsymbol{q},\dot{\boldsymbol{q}}) - \boldsymbol{K}(\boldsymbol{q}-\boldsymbol{\theta})) \end{bmatrix}, \tag{12}$$

where $\boldsymbol{x} := [\boldsymbol{\theta}, \boldsymbol{q}, \dot{\boldsymbol{q}}]^\mathsf{T}$ is the state, $\boldsymbol{u} := \dot{\boldsymbol{\theta}}$ is the new control input and $\boldsymbol{h}(\boldsymbol{q},\dot{\boldsymbol{q}}) := \boldsymbol{C}(\boldsymbol{q},\dot{\boldsymbol{q}})\dot{\boldsymbol{q}} + \boldsymbol{g}(\boldsymbol{q})$ is the nonlinear bias term.

4.2 Optimal control

We employ a direct collocation scheme to find the time series of states $\boldsymbol{x}(t)$ and control inputs $\boldsymbol{u}(t)$ (cf. Bertsekas (1997)). The optimal control problem can be stated as

$$\min_{\boldsymbol{x}(t),\boldsymbol{u}(t)} \quad \mathcal{J}(\boldsymbol{x}(t),\boldsymbol{u}(t)) \tag{13}$$

$$\text{s.t.} \quad \dot{\boldsymbol{x}}(t) = \boldsymbol{f}(\boldsymbol{x}(t),\boldsymbol{u}(t))$$

$$\boldsymbol{x}(t) \in \mathcal{X},\ \boldsymbol{u}(t) \in \mathcal{U}.$$

Here, the sets $\mathcal{X}$ and $\mathcal{U}$ denote the box constraints on the states and control inputs, respectively. As the cost function, we use the end-effector velocity

$$\mathcal{J}(\boldsymbol{x}(t),\boldsymbol{u}(t)) = -v_{EE}(\boldsymbol{x}(t)) = -\boldsymbol{J}(\boldsymbol{q}(t))\dot{\boldsymbol{q}}(t). \tag{14}$$

We formulate the optimal control problem using the Matlab interface of CasADi (cf. Andersson et al. (2019)) and solve it using Ipopt (cf. Wächter and Biegler (2006)).

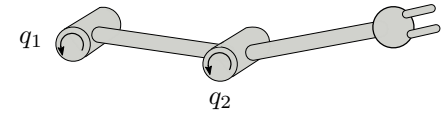

(a) Double Pendulum

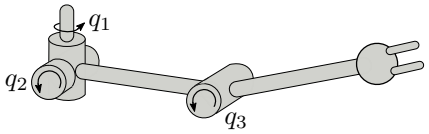

(b) Shoulder/elbow system

Fig. 9. Sketches of the two considered systems.

5. SIMULATION RESULTS

5.1 Double pendulum

We begin with the double pendulum system. The final time of the optimal control problem is $T = 1s$. The maximum motor velocity is set to $\dot{\theta}_{\max} = 2\text{rad/s}$. The stiffness matrices are set to $\boldsymbol{K} = 50\,\boldsymbol{M}(\boldsymbol{q}_0)$ for the coupled system and $\boldsymbol{K} = \mathsf{diag}([50, 50])$ for the uncoupled system. Figure 10 shows the optimal control results and Figure 11 shows a visualization of the two systems in motion. With the stiffness matrix

$$\boldsymbol{K} = \begin{bmatrix} k_1 & k_3 \\ k_3 & k_2 \end{bmatrix}, \tag{15}$$

we define the cross-coupling energy terms as

$$E_{cross,1} = k_3(\theta_2 - q_2)^2 \tag{16}$$

$$E_{cross,2} = k_3(\theta_1 - q_1)^2. \tag{17}$$

Coupled system. The system starts with a lunging motion before swinging back and forward again. The control signal is of bang-bang type for both joints. There is an important detail: The signal for the second joint always lags behind a bit. The velocity maxima of each link are reached in a consecutive manner. When viewing the energy of the system we can observe that $E_{cross,1}$ is almost zero during the last phase of the motion. This means that there is no energy transfer back to the first joint! As we can see in the plot for the energies of link 2, almost all potential energy is converted to kinetic energy. The coupling stiffness thus facilitates the energy transfer from proximal to distal links, achieving a proximo-distal sequence as described in the introduction.

Uncoupled system. The uncoupled system, on the other hand, does not show this kind of goal-directed behaviour. The excitation signal is of bang-bang type as well. However, since the oscillation behaviour is not determined by a dominant resonance frequency, the system is excited along it's multiple other frequencies resulting in a chaotic swing-up motion. This is also apparent in the energy plot of the system, which shows large oscillations from potential to kinetic energy.

5.2 Shoulder/elbow system

Next, we investigate a slightly more complex system that is a bit closer to the human arm. It consists of two limbs and three joints corresponding to shoulder adduction and internal rotation, and elbow extension. The mechanical parameters are given in Table 2. Again, we compare two similar systems, where the only difference is the stiffness matrix. The matrices are given by $\boldsymbol{K} = 75\,\boldsymbol{M}(\boldsymbol{q}_0)$, and $\boldsymbol{K} = \mathsf{diag}([75, 75])$. The final time of the optimal control problem is set to $T = 0.75\text{s}$. Figure 12 shows the optimal control solution for both systems. Figure 13 shows a visualization of the systems in motion. The system is initialized at $\boldsymbol{q}_0 = [0, 0, \pi/2]^\mathsf{T}$ with the arm extended to the side with the elbow joint at a 90-degree position. The initial motor position is chosen such that the torque generated by the springs compensate for gravity. The shoulder/elbow system has some special properties which simplify the structure of the stiffness matrix. There is no coupling between the shoulder rotation and the other two joints since the mass matrix is given by

$$\boldsymbol{M}(\boldsymbol{q}) = \begin{bmatrix} * & 0 & 0 \\ 0 & * & * \\ 0 & * & * \end{bmatrix}.$$

Here, the asterisk denotes the non-zero elements. Thus matching the scaled linearized mass matrix with a matrix $\boldsymbol{K}$ only requires two coupling elements.

Coupled system. The motion of the coupled system consists of two phases: Wind-up and acceleration. In the wind-up phase, the first joint rotates the arm back as the arm folds up. As soon as this movement comes to a standstill, the launch is initiated. Shoulder adduction and elbow extension reach their velocity limits almost simultaneously. In the last 0.25s of the motion, almost all potential energy is converted into kinetic energy again. When viewing the cross-coupling energy terms, again we can see that there is almost no energy flow back to joint 2. Similar to the double pendulum case, another proximo-distal sequence could be achieved.

Uncoupled system. In case of the uncoupled system, we can observe again a uncoordinated swing-up motion. Due to the ill-posed natural dynamics of the system with its multiple frequencies, no clear launch sequence is possible.

Table 2. Mechanical parameters of the shoulder/elbow system

Parameter	**Symbol**	**Value**
Mass Link 1	m_1	4.6 kg
Mass Link 2	m_2	4.6 kg
Mass Link 3	m_3	5 kg
Moment of Inertia Link 1	$J_{1,xx}$	0.028 kg m^2
	$J_{1,yy}$	0.0457 kg m^2
	$J_{1,zz}$	0.0457 kg m^2
Moment of Inertia Link 2	$J_{2,xx}$	0.028 kg m^2
	$J_{2,yy}$	0.0457 kg m^2
	$J_{2,zz}$	0.0457 kg m^2
Moment of Inertia Link 3	$J_{3,xx}$	0.03 kg m^2
	$J_{3,yy}$	0.0497 kg m^2
	$J_{3,zz}$	0.0497 kg m^2
Length Link 1	l_1	0.1 m
Length Link 2	l_1	0.34 m
Length Link 3	l_2	0.34 m

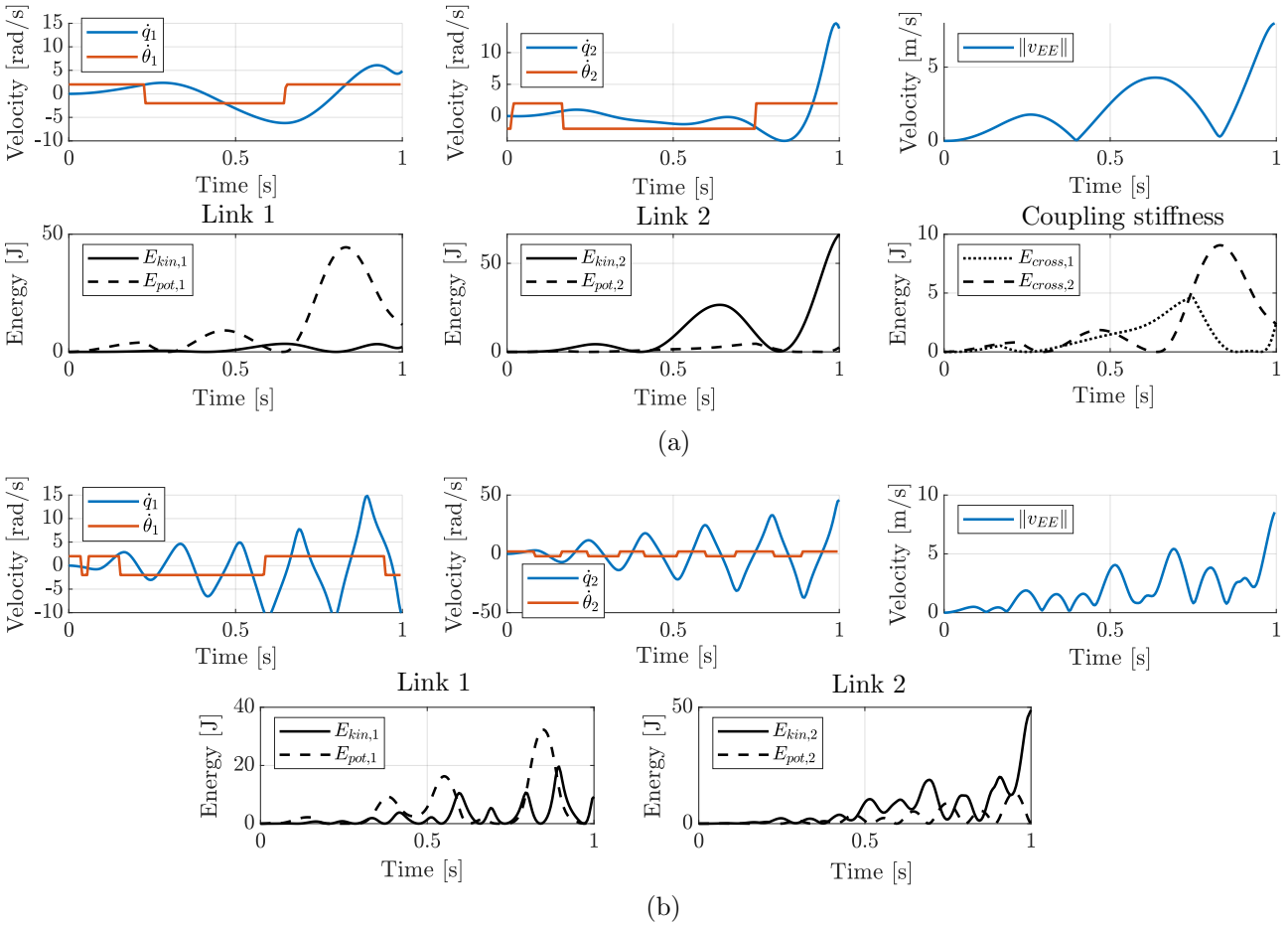

Fig. 10. Optimal control results for the double pendulum. (a) Coupled system (b) Uncoupled system.

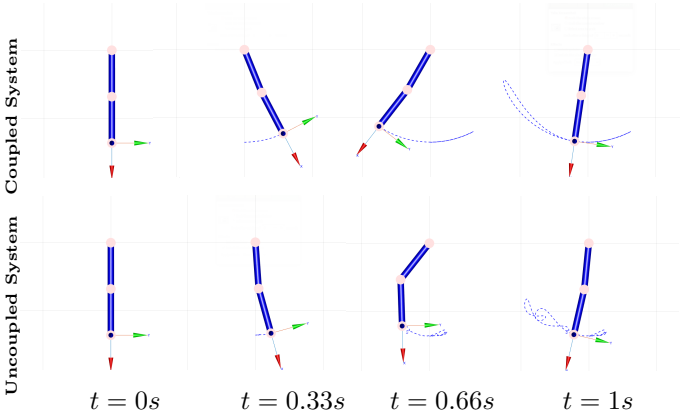

Fig. 11. Visualization of the double pendulum in motion.

6. CONCLUSION

In this paper, we showed how cross-coupling stiffness can be exploited to reshape the natural dynamics of elastic joint robots to achieve a single dominant resonance behavior. The results demonstrated that using such stiffness, the energy flow from proximal to distal parts in the kinematic chain can be intuitively controlled. Systems with coupling stiffness were able to produce natural goal-directed oscillatory motions as well as explosive movements with clear launch sequences which were not yet possible when using a diagonal stiffness.

We believe that with the advantages of cross-coupling, robots can get one step closer to the astonishing capabilities of the human musculoskeletal system and aim to realize this concept in a physical prototype.

REFERENCES

Andersson, J.A.E., Gillis, J., Horn, G., Rawlings, J.B., and Diehl, M. (2019). CasADi – A software framework for nonlinear optimization and optimal control. *Mathematical Programming Computation*, 11(1), 1–36.

Bertsekas, D.P. (1997). Nonlinear programming. *Journal of the Operational Research Society*, 48(3), 334–334.

Grebenstein, M., Albu-Schäffer, A., Bahls, T., Chalon, M., Eiberger, O., Friedl, W., Gruber, R., Haddadin, S., Hagn, U., Haslinger, R., Höppner, H., Jörg, S., Nickl, M., Nothhelfer, A., Petit, F., Reill, J., Seitz, N., Wimböck, T., Wolf, S., Wüsthoff, T., and Hirzinger, G. (2011). The DLR hand arm system. In *2011 IEEE International Conference on Robotics and Automation*, 3175–3182.

Haddadin, S., Huber, F., and Albu-Schäffer, A. (2012). Optimal control for exploiting the natural dynamics of variable stiffness robots. In *2012 IEEE International Conference on Robotics and Automation*, 3347–3354. IEEE.

Haddadin, S., Laue, T., Frese, U., Wolf, S., Albu-Schäffer, A., and Hirzinger, G. (2009). Kick it with elasticity: Safety and performance in human–robot soccer. *Robotics and Autonomous Systems*, 57(8), 761–775.

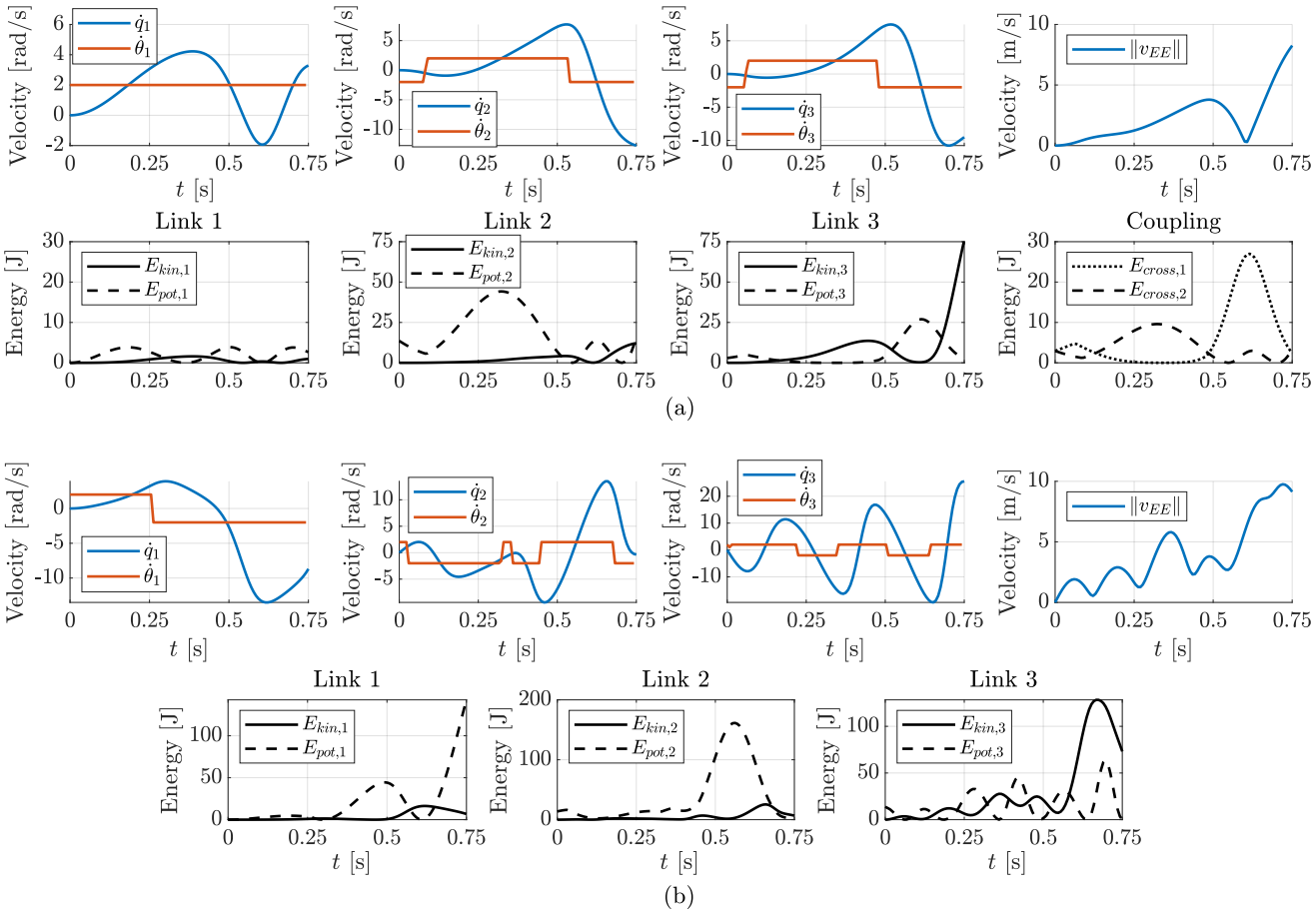

Fig. 12. Optimal control results for the shoulder/elbow system. (a) Coupled system (b) Uncoupled system.

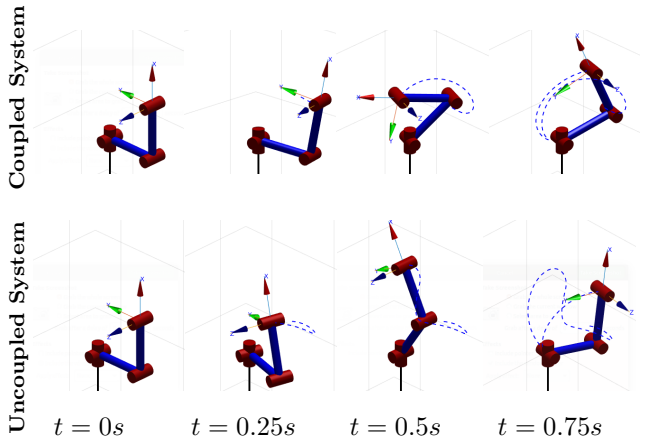

Fig. 13. Animation snapshots of the shoulder/elbow system.

Haddadin, S., Weitschat, R., Huber, F., Özparpucu, M.C., Mansfeld, N., and Albu-Schäffer, A. (2016). Optimal control for viscoelastic robots and its generalization in real-time. In *Robotics Research*, 131–148. Springer.

Heger, H. and Wank, V. (2021). Biomechanische Grundlagen des Werfens. *Sportphysio*, 9(01), 8–16.

Ossadnik, D., Yildirim, M.C., Wu, F., Swikir, A., Kussaba, H.T.M., Abdolshah, S., and Haddadin, S. (2022). BSA - Bi-Stiffness Actuation for optimally exploiting intrinsic compliance and inertial coupling effects in elastic joint robots. In *2022 IEEE/RSJ International Conference on Intelligent Robots and Systems (IROS 2022)*. IEEE.

Petit, F., Lakatos, D., Friedl, W., and Albu-Schäffer, A. (2012). Dynamic trajectory generation for serial elastic actuated robots. *IFAC Proceedings Volumes*, 45(22), 636–643.

Plooij, M., Wolfslag, W., and Wisse, M. (2017). Clutched Elastic Actuators. *IEEE/ASME Transactions on Mechatronics*, 22(2), 739–750. doi: 10.1109/TMECH.2017.2657224.

Rouse, E.J., Mooney, L.M., and Herr, H.M. (2014). Clutchable series-elastic actuator: Implications for prosthetic knee design. *The International Journal of Robotics Research*, 33(13), 1611–1625.

Spong, M. (1989). Modeling and control of elastic joint robots. *Mathematical and Computer Modelling*, 12(7), 912.

Ugurlu, B., Saglia, J.A., Tsagarakis, N.G., Morfey, S., and Caldwell, D.G. (2014). Bipedal hopping pattern generation for passively compliant humanoids: Exploiting the resonance. *IEEE Transactions on Industrial Electronics*, 61(10), 5431–5443.

Wächter, A. and Biegler, L.T. (2006). On the implementation of an interior-point filter line-search algorithm for large-scale nonlinear programming. *Mathematical programming*, 106(1), 25–57.